Synthesis of Silver Nanostructures with Controlled Shapes and Properties

BENJAMIN WILEY,[†] YUGANG SUN,[‡] AND YOUNAN XIA*,[‡]

Departments of Chemistry and Chemical Engineering, University of Washington, Seattle, Washington 98195

Received April 23, 2007

ABSTRACT

Mastery over the shape of a nanostructure enables control over its properties and usefulness for a given application. By controlling the crystallinity of the seeds from which nanostructures grow and the rate of atomic addition to seeds, we selectively produced pentagonal nanowires, cuboctahedra, nanocubes, nanobars, bipyramids, and nanobeams of silver with a solution-phase polyol synthesis. The example of nanobars illustrates how the shape of a silver nanostructure affects the color of light that it scatters. We further show how silver nanowires and nanobeams can serve as conduits for both electrons and photons.

Introduction

Silver has an array of properties that could be tuned or enhanced through the nanoscale control of morphology. For example, silver is the most popular catalyst for the oxidation of ethylene to ethylene oxide and methanol to formaldehyde.[1] In 2000, over 4×10^6 tons of these chemicals were consumed by the U.S. alone. Silver also has the highest electrical and thermal conductivity among metals, making it a popular material for electrical contacts and an additive for conducting adhesives. However, silver is perhaps most widely recognized for its unique optical properties, as manifested by its central role in photography. Photographic films are composed of silver halide crystals embedded in gelatin matrices. Upon exposure to light, silver ions are reduced into clusters of silver, creating a latent image. A critical cluster of 3–5 atoms catalyzes growth in an electron-donating developer, producing a gain of about 10^8 atoms and making the image visible.[2] A similar process has employed silver ions to produce contrast in biological tissues since the late 1800s.[3] These two applications of silver nanoparticles could be considered one of the most influential early examples of nanotechnology. More recently, silver nanoparticles have been shown to locally amplify light by 10–100 times, leading to surface-enhanced Raman scattering (SERS), with enhancement factors on the order of 10^6–10^8.[4] Several groups have reported SERS detection on the single-molecule level.[5]

Given the range of applications in which silver is important, better control of its properties would have profound economic implications. It is now well-established that, by shrinking the size of a solid particle to the nanometer regime, one can alter its chemical, electrical, mechanical, and optical properties.[6] Analogous to the way metals are machined to form macroscopic devices, tools are required to control the size and shape of metal nanostructures for a particular application. This Account is focused on the polyol synthesis, in which the nucleation and growth of silver atoms is guided in solution to produce a surprising variety of shapes. Our tools are necessarily chemical, and our goal is to refine this approach to grow nanostructures of any desired morphology.

The Polyol Synthesis

A polyol synthesis involves heating a polyol with a salt precursor and a polymeric capping agent to generate metal colloids.[7] In the case of silver nanostructures, ethylene glycol (EG), $AgNO_3$, and poly(vinyl pyrrolidone) (PVP) serve as the polyol, salt precursor, and polymeric capping agent, respectively. The reductant is continuously generated *in situ* upon heating of EG; therefore, we do not have to concern ourselves with changes in the kinetics of nanostructure growth as the reductant is added or consumed.

To delineate the relationship between the reduction rate and temperature, EG was heated in an oil bath at a given temperature for 1 h before adding $AgNO_3$ and PVP. The amount of reduced silver was then measured with atomic emission spectroscopy. As illustrated by Figure 1, a wide range of reduction rates can be accessed by merely adjusting the temperature. The temperature-dependent

Benjamin J. Wiley was born in Rochester, NY, in 1981. He received a B.S. degree in chemical engineering from the University of Minnesota in 2003 and a Ph.D. degree in chemical engineering from the University of Washington (under the guidance of Professor Younan Xia) in 2007. He is currently working as a postdoctoral fellow with Professor George M. Whitesides at Harvard University. His research interests include the modification of material properties through control over nanostructure, microstructure, and surface chemistry, as well as how such control can be applied toward the improvement of human health.

Yugang Sun was born in Shangdong, China, in 1975. He received his B.S. and Ph.D. degrees in chemistry from the University of Science and Technology of China (USTC) in 1996 and 2001, respectively. He worked as a postdoctoral research associate with Professor Younan Xia at the University of Washington until 2003 and with Professor John Rogers at the University of Illinois at Urbana–Champaign until 2006. He is now a staff scientist at the Argonne National Laboratory. His research interests include synthesis and characterization of nanostructures, micro/nanofabrication, bioanalysis, and devices for photonics and electronics.

Younan Xia was born in Jiangsu, China, in 1965. He received a B.S. degree in chemical physics from the University of Science and Technology of China (USTC) in 1987 and then worked as a graduate student on nonlinear optical materials for 4 years at the Fujian Institute of Research on the Structure of Matter, Chinese Academy of Sciences. He came to the United States in 1991, received a M.S. degree in inorganic chemistry from the University of Pennsylvania (with Professor Alan G. MacDiarmid) in 1993, and a Ph.D. degree in physical chemistry from Harvard University (with Professor George M. Whitesides) in 1996. He then worked as a postdoctoral fellow with Professors George M. Whitesides and Mara Prentiss. He moved to Seattle in 1997 and started as an Assistant Professor of Chemistry at the University of Washington. He was promoted to Associated Professor and Professor in 2002 and 2004, respectively. His research interests include nanostructured materials, nanomedicine, biomaterials, self-assembly, photonic crystals, colloidal science, microfabrication, surface modification, and electrospinning.

* To whom correspondence should be addressed. E-mail: xia@chem.washington.edu.

[†] Department of Chemical Engineering.

[‡] Department of Chemistry.

10.1021/ar7000974 CCC: $37.00
Published on Web 07/07/2007

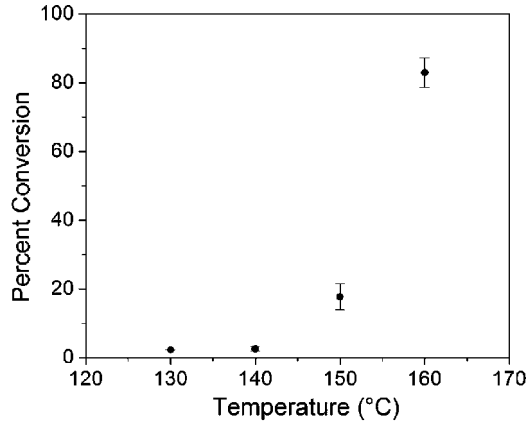

FIGURE 1. Percent of Ag^+ converted to Ag after heating with PVP in EG for 10 min at a given temperature. Each point is the average of at least three reactions, with error bars giving the standard deviation of the percent of silver reduced.

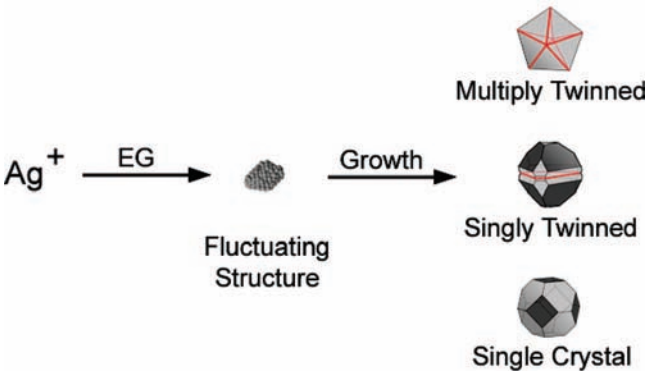

FIGURE 2. Reduction of Ag^+ ions by EG leads to the formation of nuclei. The structure of nuclei fluctuates depending upon their size and the thermal energy available. Most nuclei contain twin boundary defects because such defects enable a lower surface energy. As nuclei grow, fluctuations cease and they are stuck as a multiply twinned, singly twinned, or single-crystal seed. Different seeds then grow into nanostructures with different shapes; therefore, one must regulate the crystallinity of the seeds in a reaction to produce a specific shape.

reducing power of EG, its high boiling point, and its ability to solvate many metal precursors make the polyol synthesis an attractive method to synthesize colloidal particles of Au, Bi, Cd, Co, Cu, Pb, In, Ir, Ni, Pd, Pt, Rh, Ru, and Sn.[7–9] This flexibility facilitates the translation of the shape-control protocols developed for silver to other metals.

Within the first minute of a reaction, silver ions are reduced to atoms, which in turn come together to form nuclei. When nuclei are sufficiently small, the available thermal energy causes their structure to fluctuate, allowing defects to form or be removed depending upon their energetic favorability.[10] Most silver nuclei incorporate twin boundary defects because such defects enable a lower surface energy.[11] As nuclei grow, changes in the defect structure become too costly relative to the available thermal energy and they become stuck in a given morphology. As illustrated by Figure 2, this process results in a Boltzmann-like distribution of multiply twinned, singly twinned, and single-crystal seeds, with the 5-fold twinned decahedron being the lowest in free energy and thus the most abundant morphology.[12]

This variety of seeds grows to form nanostructures with different shapes. Our work has centered on manipulating the nucleation and growth conditions so that only one shape becomes the dominant product.

Multiply Twinned Pentagonal Nanowires

Multiply twinned decahedra are the naturally abundant seed morphology, but because of their twin defects, they are also the most reactive.[13] Silver atoms preferentially add to the twin defects of decahedra, leading to uniaxial elongation (Figure 3A). As decahedra grow into pentagonal nanorods, PVP will interact more strongly with the {100} side facets than the {111} facets at the ends of the nanowire.[14] The side surfaces of nanorods are thus passivated by PVP, while the ends remain reactive toward silver atoms. As a result, nanorods rapidly grow into nanowires tens of micrometers long. Although other seed morphologies may also nucleate and grow in the same solution, their small sizes relative to nanowires facilitate their separation by centrifugation.

To synthesize nanowires, 5 mL of EG was heated in an oil bath at 160 °C for 1 h before simultaneously injecting 3 mL of two EG solutions, one containing 48 mg of $AgNO_3$ and the other containing 48 mg of PVP (M_w = 55 000). Nanowire formation also required that the reaction solution contained 60 μM of NaCl and 3 μM of $Fe(acac)_3$; these species were added through the PVP solution.[15] If no chloride was added, the seeds rapidly aggregated to form irregular particles, suggesting that chloride adsorbs on seeds and electrostatically stabilizes them against aggregation.[16] The formation of AgCl, as indicated by the reaction solution exhibiting a white color, was not observed. Fe^{III} was added to prevent the etching of twinned seeds by chloride and oxygen. Chloride and iron are common contaminants in EG, whose concentration will vary depending upon the source; therefore, the amount added to the reaction must be adjusted in proportion to the amount initially present.

Figure 3B shows a TEM image of a sample taken from a nanowire synthesis at 30 min. At this point, the decahedral seeds had elongated to form nanorods. The nanorods rapidly grew longitudinally into nanowires tens of micrometers long by 1 h (Figure 3C). The inset shows a cross-sectional transmission electron microscopy (TEM) image of a microtomed nanowire, revealing its 5-fold twinned crystal structure and pentagonal profile. To test our hypothesis about the role of PVP in nanowire formation, we sonicated silver nanowires first with a dithiol linker and then with gold nanoparticles. Figure 3D shows that the {111} facets at the ends of nanowires were decorated with gold nanoparticles but not the {100} facets on the sides of the wires, which should have been blocked with PVP.

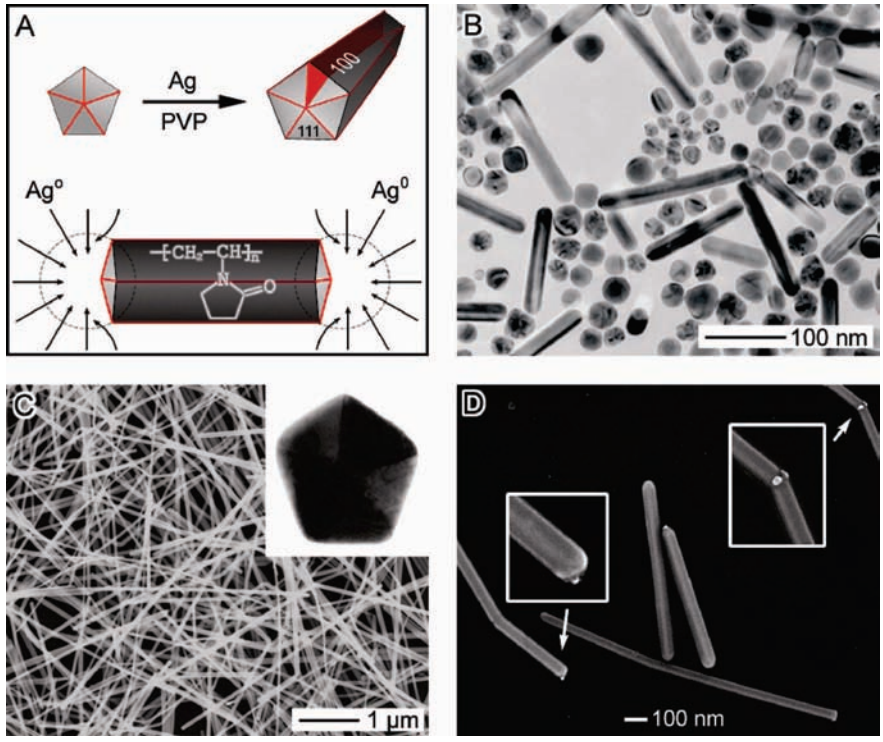

FIGURE 3. (A) Once twinned decahedral seeds lengthened into rods. PVP selectively adsorbed on the {100} side facets so that Ag atoms could only add to the {111} facets at the ends of each rod. (B) After 30 min, TEM shows the presence of nanorods along with twinned particles in a reaction to which $Fe(acac)_3$ and NaCl were added. (C) SEM image of nanowires obtained at 1 h. (D) SEM image of as-prepared silver nanowires that were sonicated with a dithiol linker and then gold nanoparticles. This image indicates that gold nanoparticles stuck to the ends of wires and freshly cleaved surfaces but not to the sides of the wires coated with PVP.

Single-Crystal Nanocubes and Cuboctahedra

One must prevent the formation of decahedral seeds to obtain nanostructures other than nanowires in high yields. We accomplished this by following the same procedure as the nanowire synthesis but without adding any iron species. In the presence of Cl^- and air, the higher reactivity of seeds with twin defects caused them to be selectively etched away.[17] For oxidative etching to occur, the concentration of iron species should be below 0.2 μM.

Etching could be monitored by the reaction color. Because silver nanoparticles absorb blue light at $\lambda \approx$ 400 nm, red and green combine to give the reaction a yellow color at 10 min (Figure 4A). Figure 4B shows a TEM image of a reaction sample at 10 min, in which most particles were twinned. However, rather than grow into silver nanowires, these twinned particles were etched away. After 7 h, the solution became clear (Figure 4C) and very few silver particles could be found with TEM. The UV–vis spectra of reaction samples in Figure 4D further illustrate that the plasmon resonance peak intrinsic to silver nanoparticles was present at 10 min but gradually disappeared as twinned particles were etched away.

The yellow color returned at about 24 h and grew in intensity until 44 h, at which time the TEM of a sample showed that the particles were all single crystals (Figure 5A). After this point, the single crystals rapidly grew in size. Scanning electron microscopy (SEM) of the reaction product at 46 h showed the single crystals to be 80 nm cuboctahedra (Figure 5B). If the water initially present in EG was removed by flowing dry nitrogen through the reaction flask for the first 8 min of preheating, the reaction time was cut in half.[18] The TEM image in Figure 5C shows that the single crystals subsequently produced by 22 h were nanocubes, 25 nm in edge length. After 24 h, these nanocubes grew to be 80 nm in size while retaining relatively sharp corners (Figure 5D). Although a nanocube has a higher surface energy than a cuboctahedron of the same size, its formation may be favored at relatively high rates of atomic addition {111} facets because of the adsorption of PVP to {100} facets. Thus, when the rate of atomic addition to different facets is controlled, single-crystal seeds can be grown into different shapes.

Studies of silver catalysts have shown that a higher defect density leads to greater activity for oxidation reactions.[19] We propose that it is the higher density of defects on the surface of twinned seeds that led to their greater activity for oxidative etching. Our experiments indicate that both Cl^- and O_2 were required for oxidative etching of twinned seeds.[17] If the reaction was performed under argon rather than air, the twinned particles present at 10 min grew to form multiply twinned nanowires in 1.5 h. Without the addition of Cl^-, the Ag precursor was quickly reduced to form multiply twinned particles,

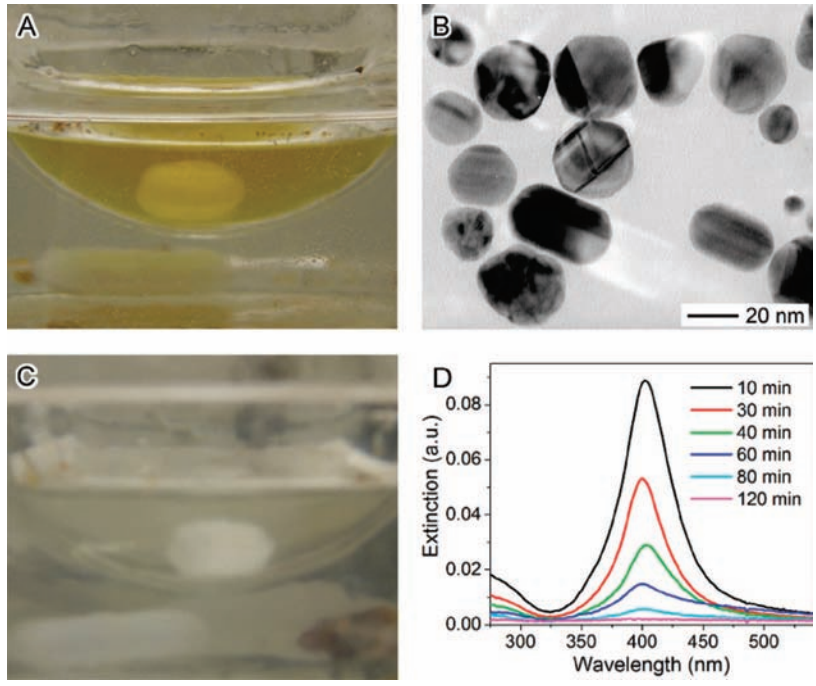

FIGURE 4. (A and C) Photographs of a reaction solution at 10 min and 7 h, respectively, showing the formation and subsequent etching of silver nanoparticles in the presence of NaCl and air (molar ratio of Ag/Cl = 4.2×10^5). (B) TEM image showing that mostly twinned nanoparticles were present in the reaction at 10 min. (D) UV–vis spectra of six samples taken from the same reaction between 10 and 120 min, further confirming the initial formation and subsequent dissolution of twinned silver nanoparticles.

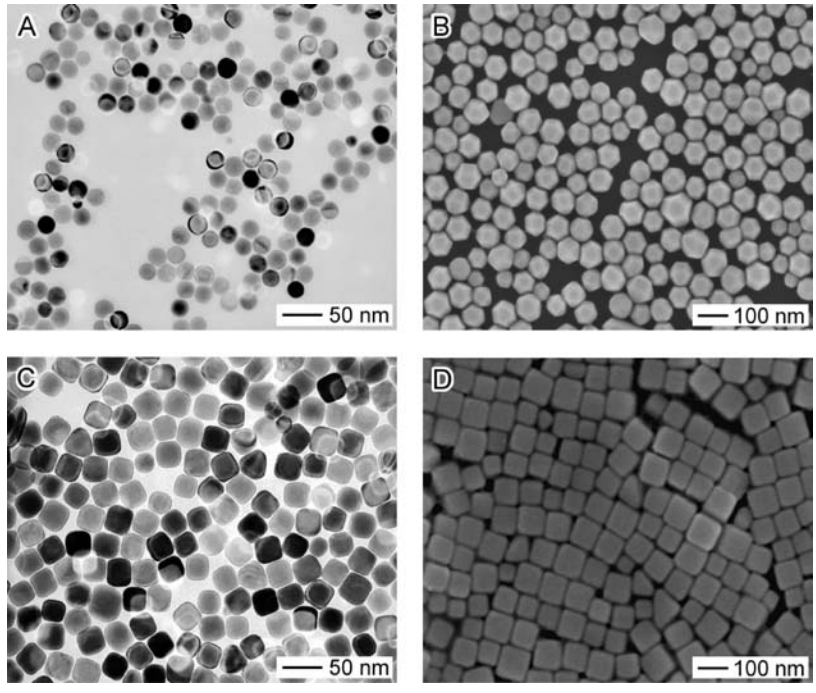

FIGURE 5. (A) Second round of nucleation and growth produced single-crystal spheres ~ 20 nm in diameter, as illustrated by this TEM image of a sample taken at 44 h. (B) SEM shows single crystals grew to form truncated nanocubes approximately 80 nm in diameter after 46 h. (C) Faster growth of single crystals resulted in the formation of nanocubes about 25 nm in edge length by 20 h. (D) Nanocubes grew to about 80 nm in edge length by 22 h.

100–300 nm in size, in less than 1 h. Incidentally, it is widely recognized that Cl^- accelerates the corrosion of metals.[20] The corrosion of steel in salt water is a well-known example. Although it seems likely that the corrosive effect of Cl^- helped to etch twinned seeds, as in the corrosion of steel, the role of Cl^- is not completely understood. Nonetheless, because oxidative etching plays a role in the polyol synthesis of palladium, platinum, and rhodium nanostructures, it can be considered a general tool to control both crystallinity and shape.[21–23]

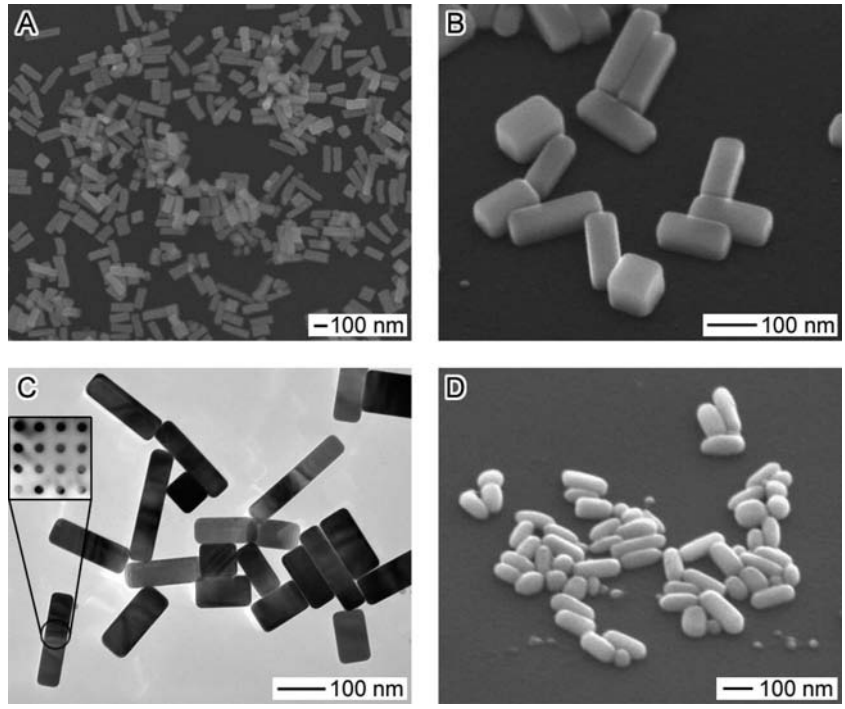

FIGURE 6. (A) SEM image of the Ag nanobars produced when NaCl was substituted with NaBr. (B) SEM image of the same sample tilted by 45°. (C) TEM image of the silver nanobars. The inset is a convergent beam electron diffraction pattern, indicating that the nanobars are single crystals bound by (100) facets. (D) SEM of nanorice at a 45° tilt.

Single-Crystal Nanobars and Nanorice

If NaCl was substituted with 60 μM NaBr and the oil bath temperature was lowered to 155 °C, the reaction produced silver nanobars in 1 h.[24] PVP and $AgNO_3$ concentrations remained the same as in the synthesis of nanowires. The formation of AgBr was not observed at this NaBr concentration. Figure 6A shows a SEM image of the product, which contained both nanocubes and nanobars with a range of aspect ratios. In Figure 6B, where the sample has been tilted by 45°, it appears that nanobars are both narrower and thinner than nanocubes in the same sample. Figure 6C shows a TEM image of silver nanobars. Convergent beam electron diffraction on several nanobars gave patterns identical to the one included as an inset, which shows diffraction from the (100) planes. Because all sides of the nanobars meet at right angles, this pattern proves that nanobars, similar to nanocubes, are single crystals bound on all sides by {100} facets. Storage of nanobars in a 5 wt % aqueous solution of PVP for 1 week resulted in their transformation into single-crystal nanorice with rounded corners and edges (Figure 6D).

Given that every side of the nanobar has the same surface energy, it is not clear why nanobars grew anisotropically. Obviously, the most important ingredient for promoting the growth of nanobars is bromide. Higher concentrations of bromide also promote anisotropic growth in the synthesis of Pd nanobars and nanorods (Br/Pd $\approx$ 30), as well as gold nanorods (Br/Au $\approx$ 190).[25,26] Although questions remain as to its mechanism of action, it is interesting that bromide generally induces anisotropic growth among these noble metals.

Singly Twinned Right Bipyramids

To selectively produce seeds with a single twin plane, the degree of etching must be moderated so that the most reactive multiply twinned seeds are etched away but seeds with a single twin plane remain intact.[27] This is accomplished by reducing the amount of bromide by half relative to the nanobar reaction, to 30 μM. Again, the PVP and $AgNO_3$ concentrations were the same as in the nanowire synthesis, and the oil bath temperature was 160 °C.

Figure 7A shows a high-resolution (HR)TEM image of a single twinned seed, many of which could be found in a reaction sample taken at 1.5 h. Atomic lattice fringes reflect across the twin plane, with the 2.4 Å fringe spacing confirming that the twin defect is on the (111) plane. A zoomed-out view of the same particle is given in the inset to illustrate its spherical profile and bisection by a twin plane. Figure 7B shows a 40 nm right bipyramid present in the reaction at 2.5 h. It is tilted 45° to show its bisection by a twin plane, with each half being equivalent to the corner of a nanocube. Right bipyramids grew to be 75 nm (Figure 7C) or 150 nm (Figure 7D) in edge length in a reaction stopped at 3 or 5 h, respectively. The inset in Figure 7C shows a typical electron diffraction pattern obtained from a single right bipyramid, with the beam perpendicular to the substrate. The spot array is characteristic of diffraction from the (100) zone axis and indicates that the bipyramid lies with a (100) facet flush with the substrate. Because every facet on the bipyramid is identical, we can conclude that the bipyramid, similar to the nanocube, is also bound by {100} facets.

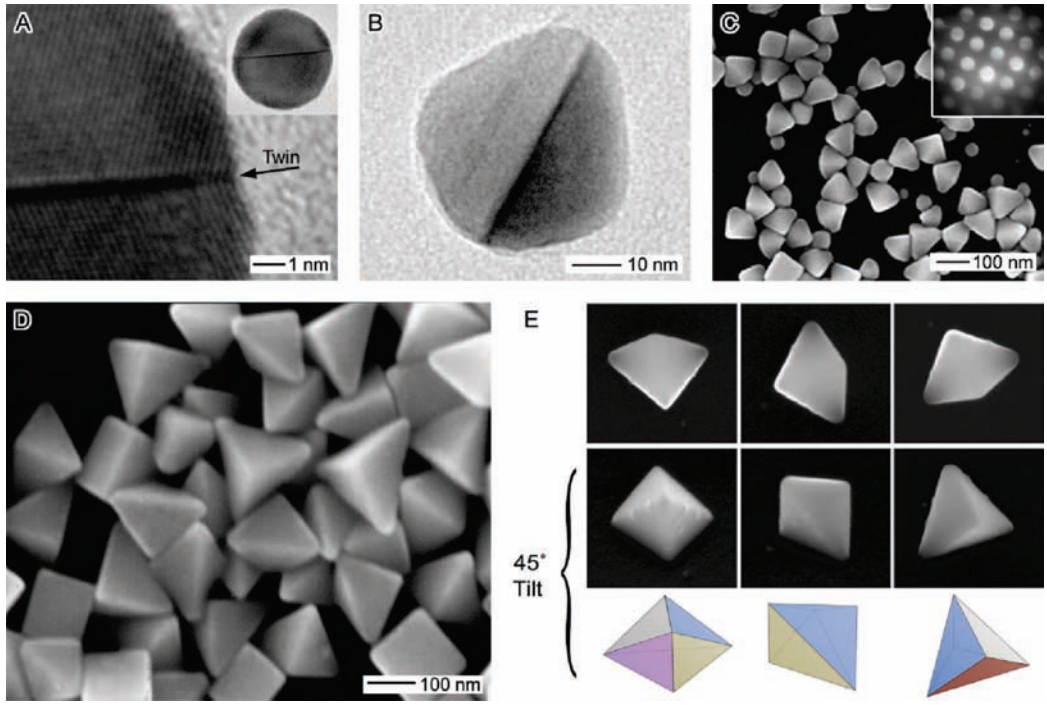

FIGURE 7. (A) HRTEM image of a singly twinned seed present at 1.5 h in a reaction to which NaBr was added at a ratio of Ag/Br = 8.4 × 10^5. Lattice fringes reflect across the (111) twin plane denoted by an arrow. The inset illustrates the spherical profile of the particle and bisection by a twin plane. (B) TEM of a right bipyramid ~40 nm in edge length taken from the reaction at 2.5 h. It is tilted by 45° to show its bisection by a twin plane. (C and D) SEM images of bipyramids approximately 75 and 150 nm in edge length. The electron diffraction pattern from a single bipyramid, shown as an inset in C, indicates that the bipyramid is bound by (100) facets. (E) SEM images of a right bipyramid at different rotations from above (top panels) and at a 45° tilt. CAD models of a right bipyramid are shown for a comparison.

To depict its shape and orientation more clearly, Figure 7E shows SEM images of a single right bipyramid from above and from 45° at three different rotations. The tilted bipyramids are compared with computer-aided design (CAD) models of right bipyramids at identical orientations. It is impossible to visualize the right bipyramid from the top view alone, but from 45°, it becomes clear that one half of the bipyramid, which can be thought of as a corner of a cube, points up and away from the substrate. The other half points toward and has one of its sides in contact with the substrate. The selective enlargement of (100) surfaces on the twinned seed to make a right bipyramid is consistent with our nanocube and nanowire syntheses, in which the selective capping of {100} facets by PVP and relatively fast growth of other facets led to the formation of nanostructures bound by {100} facets.

Singly Twinned Nanobeams

Seeds with a single twin could also be grown slowly over 24 h to form silver nanobeams.[28] Silver nanobeams are so named because they have a cross-sectional aspect ratio similar to that of a beam of wood. In comparison to the synthesis of right bipyramids, the concentration of $AgNO_3$ and PVP was doubled and the temperature was lowered by 12°, while the concentration of NaBr was kept the same. Although the concentration of the silver precursor was doubled, the lower reaction temperature resulted in a slower reduction rate.

Figure 8A shows a SEM image of the silver nanobeams produced at 24 h. Their widths ranged from about 17 to 70 nm; about 85% had widths less than 40 nm. On the basis of this image and others, we estimate 95% of the nanobeams were over 3 μm long and approximately 60% were over 10 μm. Under TEM (Figure 8B), nanobeams displayed striations of contrast distinct from the 2-fold contrast characteristic of pentagonal nanowires.[14] When a nanobeam is viewed at 65° from normal by SEM (Figure 8C), it has a rounded profile. The microtomed nanobeam cross-sections in Figure 8D appear to be bisected by a single twin plane, suggesting that the nanobeams grew from singly twinned seeds. The nanobeam in the lower left of this image, which is more closely aligned with the electron beam, is 38 nm wide and 27 nm thick; hence, the width/thickness ratio, W/T, is 1.4. Correlated SEM and atomic force microscopy measurements gave aspect ratios consistent with this TEM analysis.

Tuning Plasmons with Nanobars and Nanorice

Morphological control provides a powerful tool for the creation of nanostructures with unique spectral signatures for optical labeling and sensing applications.[29] Silver nanoparticles have a particular advantage in labeling applications because their scattering cross-section is an order of magnitude larger than that of gold, they are equivalent to 10^6 fluorescein molecules in light-producing power, and they do not photobleach.[30] Nanobars and nanorice illustrate how the optical properties of a silver nanostructure are determined by its shape.[24] The normalized scattering spectra of individual nanobars are plotted in Figure 9A, with insets giving SEM images of the nanobars from which scattered

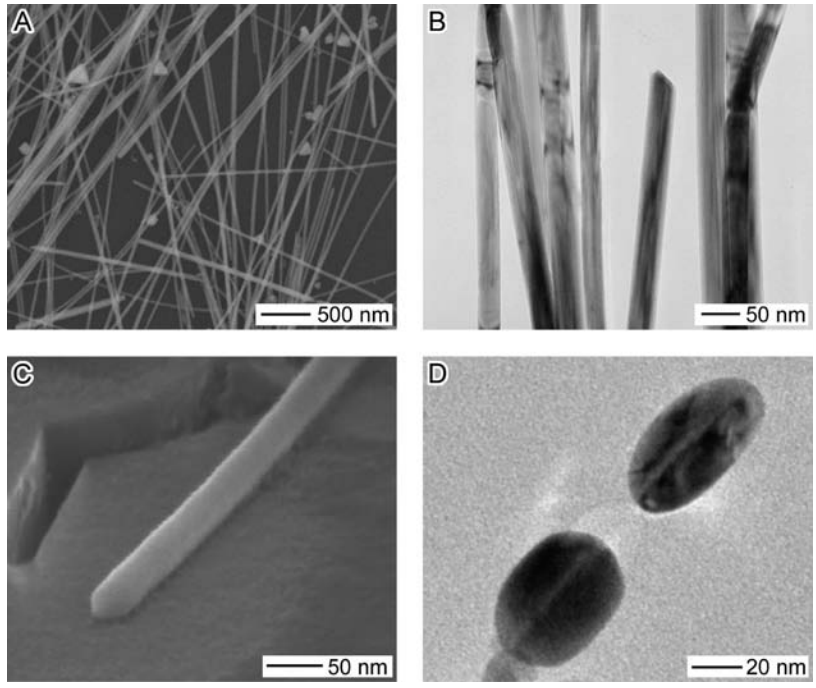

FIGURE 8. (A) SEM and (B) TEM images of Ag nanobeams. In comparison to the synthesis of right bipyramids, the concentration of $AgNO_3$ and PVP was doubled and the temperature was lowered by 12°. (C) SEM image of a nanobeam tilted at 65° relative to the electron beam (the scale bar only applies to the horizontal axis). (D) TEM image of a microtomed sample of Ag nanobeams showing their cross-sectional profile and bisection by a twin plane.

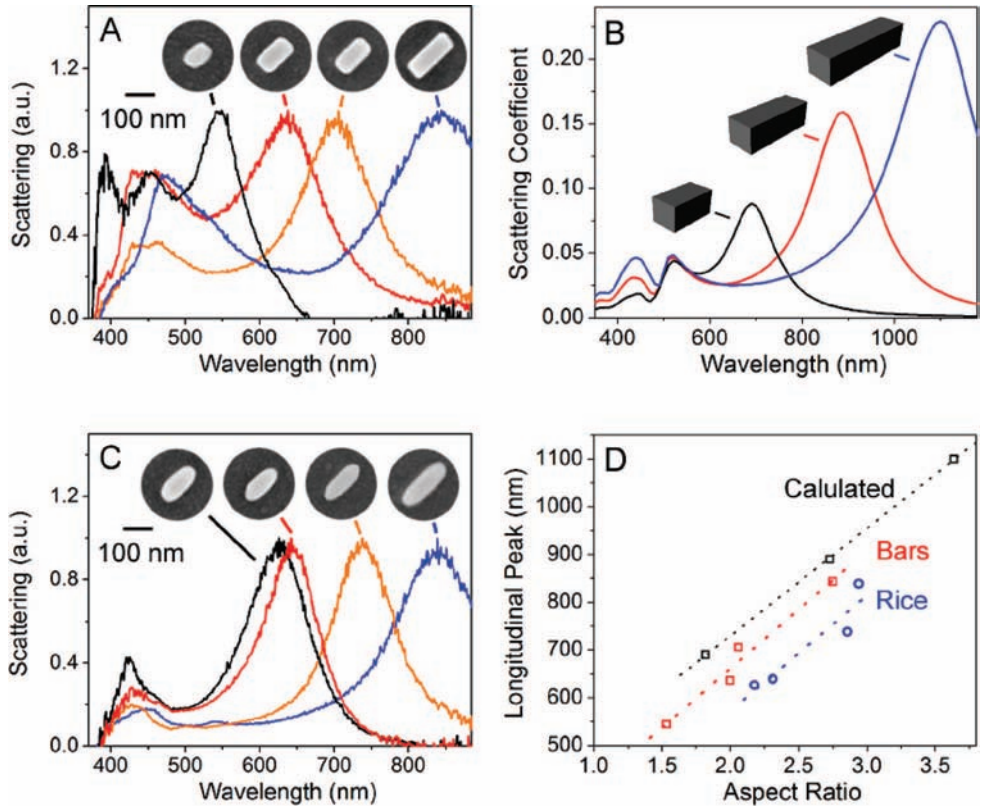

FIGURE 9. (A) SEM images of individual Ag nanobars with their corresponding normalized scattering spectra. (B) DDA calculated scattering spectra of nanobars, 100, 150, and 200 nm in length, keeping width = 55 nm and height = 50 nm. (C) SEM images of individual nanorice with their corresponding normalized scattering spectra. (D) Plot of the longitudinal plasmon peak location versus the aspect ratio.

light was collected. For each nanobar, the position of the transverse resonance peak (from light polarized along the short axis) stayed in the blue region of the visible spectrum. In contrast, the longitudinal resonance peak shifted from the visible into the near infrared (NIR) as the nanobar aspect ratio increased.

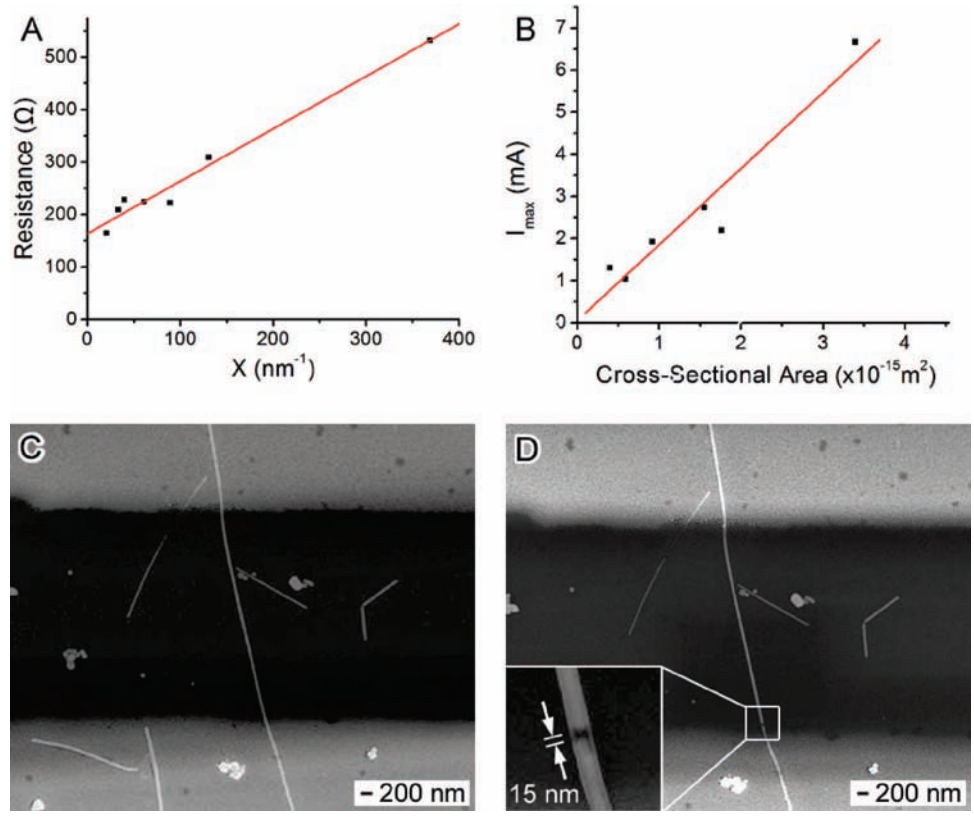

FIGURE 10. (A) Plot of the resistance of nanobeams versus $X = \rho_0(L/0.56W^2)(1 + (\lambda/0.75W))$ to give $\lambda = 15$ nm. The straight line fit has a slope of unity, and the y intercept gives a contact resistance, $R_c = 164\ \Omega$. Here, λ is a characteristic thickness at which the resistivity deviates from bulk silver and is determined by the bulk mean free path, l, the shape, and surface scattering. (B) Current at failure, I_{max}, is proportional to the cross-sectional area of the nanobeams, with a slope representing a well-defined maximum current density of approximately 1.8×10^8 A cm^{-2}. (C and D) SEM images of a nanobeam before and after testing for the maximum current that it could support, with the inset showing the 15 nm gap that formed as a result.

The resonance peaks of synthesized nanobars are blue-shifted relative to spectra calculated with the discrete dipole approximation (DDA), shown in Figure 9B.[31] We suspected that this shift was caused by the DDA calculations using nanobar models with sharper corners and edges than synthesized ones. To explore the effect of sharpness on the resonance peak position, we looked at the spectra of individual nanorice. The normalized scattering spectra of nanorice with different aspect ratios are plotted in Figure 9C, with insets showing SEM images of the nanorice from which the scattered light was collected. Similar to nanobars, the position of the transverse resonance peak did not change significantly for nanorice with different aspect ratios and the longitudinal resonance peak red-shifted with an increasing aspect ratio. However, the rounded corners and edges of nanorice caused both the transverse and longitudinal resonance peaks to be blue-shifted relative to those of nanobars.

To compare the scattering spectra of individual nanobars and nanorice with the DDA-predicted spectra from ideal nanobars, we plotted the longitudinal resonance peak position versus the aspect ratio in Figure 9D. For each nanostructure, the longitudinal resonance red-shifts linearly with an increasing aspect ratio. The DDA calculations on nanobars with ideal corner and edge sharpness exhibit the most red-shifted resonance at a given aspect ratio, followed by nanobars and nanorice. Thus, the optical properties of a silver nanostructure can be tuned by controlling both anisotropy and corner sharpness.

Electron Transport through Nanobeams

The well-defined dimensions, smooth surface, and crystallinity of nanobeams make them promising candidates for studying the effects of size on electron transport.[28] The effective resistivity, ρ, of a nanoscale metal film or wire is higher than the bulk value, ρ_0, because of surface scattering. If we theoretically reduce the cross-sectional area, $A \equiv a^2$, of wires with a given shape, the correction to ρ should initially be linear in the surface/volume ratio, a^{-1}, i.e., $\rho = \rho_0(1 + \lambda/a)$, where λ is a characteristic length scale and $\lambda/a \ll 1$.[32] The scale λ is set by the bulk mean free path, l, the shape, and the details of the surface scattering. In addition to the resistance of the nanobeam, we anticipate a contact resistance, R_c. Assuming for simplicity that R_c is the same for every device and putting $A \approx \pi WT/4 \approx 0.56W^2$ and $a = A^{1/2} \approx 0.75W$ for the nanobeams, we obtain

$$R - R_c \approx \rho\frac{L}{A} \approx \rho_0\frac{L}{0.56W^2}\left(1 + \frac{\lambda}{0.75W}\right) \qquad (1)$$

To see how well this describes the nanobeams, we plot values of R against values of the expression on the right

hand side of eq 1, calculated using the bulk value of $\rho_0 = 1.6\ \mu\Omega$ cm for silver and a value of λ that was adjusted to give the best fit to a line of slope unity. The result is shown in Figure 10A, with $\lambda = 15$ nm and $R_c = 164\ \Omega$. The scatter about the line could be explained by random variations in the resistance of the contacts. Because, according to eq 1, even our thinnest nanobeams, with $W \approx 20$ nm, have a resistivity only twice that of bulk silver, it appears that nanobeams largely retain the electrical conductivity of the bulk material.

The current at failure, I_{max}, is plotted versus the cross-sectional area, A, in Figure 10B. The data is consistent with $I_{max} \propto A$, with a slope representing a well-defined maximum current density of 1.8×10^8 A cm^{-2}. This is comparable to the highest current densities reported for multiwalled carbon nanotubes ($\sim 10^9$ A cm^{-2}).[33] Failure occurred by the formation of a gap about 15 nm wide in the nanobeam, as can be discerned in the SEM images of a nanobeam before and after testing for the maximum current density (parts C and D of Figure 10). The formation of such gaps suggests this procedure as a simple way to fabricate nanoscale electrodes separated by a few nanometers that, unlike previous methods, completely circumvents the need for lithography.[34]

Photon Transport through Nanowires

Figure 11A shows that if laser light is focused on one end of a silver nanowire, it is re-emitted at the opposite end, even around curves with a radius of curvature of 4 μm.[35] The momentum of a photon is not the same as that of a propagating plasmon; therefore, scattering is required to provide an additional wave vector for coupling light into a propagating plasmon. This condition is met at the sharp ends of the nanowire, where light can scatter axially into propagating plasmon modes. Propagating plasmons incident upon the sharp ends of the wire can in turn re-emit as photons. Figure 11B illustrates that if a nanowire had sharp bends or kinks, light leaked out at the kink sites. These kinks have radii of curvature below the diffraction limit and thus, similar the ends of the nanowire, scatter propagating plasmons into photons. Light can also couple from one nanowire to another. Figure 11C demonstrates this effect, in which light is observed not only at the intersections but also at the ends of adjacent nanowires, indicating that light is coupled between them.

Although dielectrics and semiconductors can guide and propagate light over longer distances, silver nanowires can focus and guide light at the nanoscale via plasmon propagation. Future studies will focus on the incorporation of nanowire waveguides into nanoscale optical circuits and sensors.[36]

Conclusion

Controlling the crystallinity of a seed is not only a necessary prerequisite for producing a given nanostructure in high yield but also an effective tool to access a wide range of shapes with only one synthetic process. A challenge for future syntheses is to form new seed

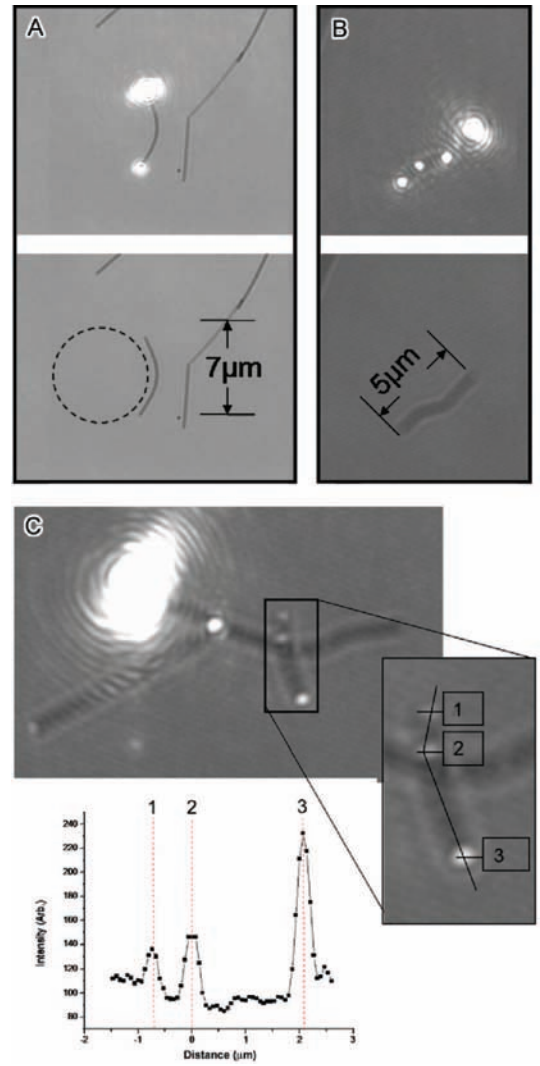

FIGURE 11. Optical micrographs showing plasmon excitation, propagation, and emission for Ag nanowires. The brightest point in each image is scattered light from the incident laser. (A) Light propagated as a plasmon along a nanowire of 7 μm long with a radius of curvature of 4 μm and emitted from the other end. (B) Sharp kinks of a wire caused the radiation of light in addition to the end. (C) Excitation at the far left end of a nanowire produces emission at both the junctions and ends of adjacent, coupled nanowires. The inset gives the emission intensity profile along an adjacent nanowire.

morphologies that do not represent an energy minimum for a given crystal structure but, instead, are induced to form by the presence of or reactions with chemical species added to the reaction. To this end, a combination of high-resolution mass spectroscopy and theoretical calculations will expedite an understanding of nuclei formation,[37] as well as the influence of chemical species on nuclei morphology.

By exploring the properties of silver nanostructures, we can gain a better understanding of the interaction between light and electrons at the nanoscale. Although we chose the example of nanobars and nanorice to illustrate the effect of shape on color, this does not do justice to the fascinating and complex relationship between the shape of a nanostructure and its optical properties, as well as

how shape affects signal intensity in molecular-sensing platforms.[29] The fact that silver nanowires are excellent conductors of both electrons and photons opens up intriguing possibilities for electro-optical devices that have yet to be explored.

This work has been supported in part by NSF, ONR, and a Fellowship from the David and Lucile Packard Foundation. Y.X. is an Alfred P. Sloan Research Fellow and a Camille Dreyfus Teacher Scholar. Electron microscopy studies were performed at the Nanotech User Facility, a member of the National Nanotechnology Infrastructure Network (NNIN) funded by NSF. B.W. has been supported by an IGERT and a Nanotech Fellowship from the University of Washington (UW) Center for Nanotechnology. We thank our collaborators for their contributions to this research.

References

(1) Nagy, A.; Mestl, G. High Temperature Partial Oxidation Reactions over Silver Catalysts. *Appl. Catal., A* **1999**, *188*, 337–353.
(2) Belloni, J. Photography: Enhancing Sensitivity by Silver-Halide Crystal Doping. *Radiat. Phys. Chem.* **2003**, *67*, 291–296.
(3) Newman, R.; Jasani, B. Silver Development in Microscopy and Bioanalysis: Past and Present. *J. Pathol.* **1998**, *186*, 119–125.
(4) Haynes, C. L.; McFarland, A. D.; Van Duyne, R. P. Surfac-Enhanced Raman Spectroscopy. *Anal. Chem.* **2005**, *77*, 338A–346A.
(5) Nie, S.; Emory, S. R. Probing Single Molecules and Single Nanoparticles by Surface-Enhanced Raman Scattering. *Science* **1997**, *275*, 1102–1106.
(6) Ozin, G. A.; Arsenault, A. C. *Nanochemistry: A Chemical Approach to Nanomaterials*; RSC Publishing: Cambridge, U.K., 2006.
(7) Fievet, F.; Lagier, J. P.; Figlarz, M. Preparing Monodisperse Metal Powders in Micrometer and Submicrometer Sizes by the Polyol Process. *MRS Bull.* **1989**, *14*, 29–34.
(8) Wang, Y.; Xia, Y. Bottom–Up and Top–Down Approaches to the Synthesis of Monodispersed Spherical Colloids of Low Melting-Point Metals. *Nano Lett.* **2004**, *4*, 2047–2050.
(9) Bonet, F.; Delmas, V.; Grugeon, S.; Urbina, R. H.; Silvert, P. Y.; Tekaia-Elhsissen, K. Synthesis of Monodisperse Au, Pt, Pd, Ru and Ir Nanoparticles in Ethylene Glycol. *Nanostruct. Mater.* **1999**, *11*, 1277–1284.
(10) Ferrando, R.; Baletto, R. Structural Properties of Nanoclusters: Energetic, Thermodynamic, and Kinetic Effects. *Rev. Mod. Phys.* **2005**, *77*, 371–423.
(11) Ajayan, P. M.; Marks, L. D. Quasimelting and Phases of Small Particles. *Phys. Rev. Lett.* **1998**, *60*, 585–587.
(12) Marks, L. D. Experimental Studies of Small Particle Structures. *Rep. Prog. Phys.* **1994**, *57*, 603–649.
(13) Lofton, C.; Sigmund, W. Mechanisms Controlling Crystal Habits of Gold and Silver Colloids. *Adv. Funct. Mater.* **2005**, *15*, 1197–1208.
(14) Sun, Y.; Mayers, B.; Herricks, T.; Xia, Y. Polyol Synthesis of Uniform Silver Nanowires: A Plausible Growth Mechanism and the Supporting Evidence. *Nano Lett.* **2003**, *3*, 955–960.
(15) Wiley, B.; Sun, Y.; Xia, Y. Polyol Synthesis of Silver Nanostructures: Control of Product Morphology with Fe(II) or Fe(III) Species. *Langmuir* **2005**, *21*, 8077–8080.
(16) Goia, D. V. Preparation and Formation Mechanisms of Uniform Metallic Particles in Homogeneous Solutions. *J. Mater. Chem.* **2004**, *14*, 451–458.
(17) Wiley, B.; Herricks, T.; Sun, Y.; Xia, Y. Polyol Synthesis of Silver Nanoparticles: Use of Chloride and Oxygen To Promote the Formation of Single-Crystal, Truncated Cubes and Tetrahedrons. *Nano Lett.* **2004**, *4*, 1733–1739.
(18) Chen, J.; Saeki, F.; Wiley, B.; Cang, H.; Cobb, M. J.; Li, Z.-Y.; Au, L.; Zhang, H.; Kimmey, M. B.; Li, X.; Xia, Y. Gold Nanocages: Bioconjugation and Their Potential Use as Optical Imaging Contrast Agents. *Nano Lett.* **2005**, *5*, 473–477.
(19) Buatier de Moneot, F.; Cupolillo, A.; Valbusa, U.; Rocca, M. O_2 Dissociation on Ag(001): The Role of Kink Sites. *Chem. Phys. Lett.* **1997**, *270*, 345–350.
(20) Bradford, S. A. *Corrosion Control*, 2nd ed.; CASTI Publishing: Edmonton, Canada, 2001; pp 1–51.
(21) Xiong, Y.; Chen, J.; Wiley, B.; Xia, Y.; Aloni, S.; Yin, Y. Understanding the Role of Oxidative Etching in the Polyol Synthesis of Pd Nanoparticles with Uniform Shape and Size. *J. Am. Chem. Soc.* **2005**, *127*, 7332–7333.
(22) Chen, J.; Herricks, T.; Xia, Y. Polyol Synthesis of Platinum Nanostructures: Control of Morphology through Manipulation of Reduction Kinetics. *Angew. Chem., Int. Ed.* **2005**, *44*, 2589–2592.
(23) Zettsu, N.; McLellan, J. M.; Wiley, B.; Yin, Y.; Li, Z.-Y.; Xia, Y. Rhodium Multipods: Synthesis, Stability, Surface Plasmonic Properties, and Their Use as Substrates for Surface-Enhanced Raman Scattering. *Angew. Chem., Int. Ed.* **2006**, *45*, 1288–1292.
(24) Wiley, B. J.; Chen, Y.; McLellan, J. M.; Xiong, Y.; Li, Z.-Y.; Ginger, D. S.; Xia, Y. Synthesis and Optical Properties of Silver Nanobars and Nanorice. *Nano Lett.* **2007**, *7*, 1032–1036.
(25) Xiong, Y.; Cai, H.; Wiley, B. J.; Wang, J.; Kim, M. J.; Xia, Y. Synthesis and Mechanistic Study of Palladium Nanobars and Nanorods. *J. Am. Chem. Soc.* **2007**, *129*, 3665–3675.
(26) Murphy, C. J.; Gole, A. M.; Hunyadi, S. E.; Orendorff, C. J. One-Dimensional Colloidal Gold and Silver Nanostructures. *Inorg. Chem.* **2006**, *45*, 7544–7554.
(27) Wiley, B.; Xiong, Y.; Li, Z.-Y.; Xia, Y. Right Bipyramids of Silver: A New Shape Derived from Single Twinned Seeds. *Nano Lett.* **2006**, *6*, 765–768.
(28) Wiley, B.; Wang, Z.; Wei, J.; Yin, Y.; Cobden, D. H.; Xia, Y. Synthesis and Electrical Characterization of Silver Nanobeams. *Nano Lett.* **2006**, *6*, 2273–2278.
(29) Wiley, B.; Im, S.-H.; Li, Z.-Y.; McLellan, J. M.; Siekkinen, A.; Xia, Y. Maneuvering the Surface Plasmon Resonance of Silver Nanostructures through Shape-Controlled Synthesis. *J. Phys. Chem. B* **2006**, *110*, 15666–15675.
(30) Yguerabide, J; Yguerabide, E. E. Light-Scattering Submicroscopic Particles as Highly Fluorescent Analogs and Their Use as Tracer Labels in Clinical and Biological Applications. *Anal. Biochem.* **1998**, *262*, 137–156.
(31) Yang, W.-H.; Schatz, G. C.; Van Duyne, R. P. Discrete Dipole Approximation for Calculating Extinction and Raman Intensities for Small Particles with Arbitrary Shapes. *J. Chem. Phys.* **1995**, *103*, 869–875.
(32) Dingle, R. B. The Electrical Conductivity of Thin Wires. *Proc. R. Soc. London, Ser. A* **1950**, *201*, 545–560.
(33) Bourlon, B.; Glattli, D. C.; Placais, B.; Berroir, J. M.; Milko, C.; Forro, L.; Bachtold, A. Geometrical Dependence of High-Bias Current in Multiwalled Carbon Nanotubes. *Phys. Rev. Lett.* **2004**, *92*, 026804.
(34) Park, H.; Lim, A. K. L.; Alivisatos, A. P.; Park, J.; McEuen, P. L. Fabrication of Metallic Electrodes with Nanometer Separation by Electromigration. *Appl. Phys. Lett.* **1999**, *75*, 301–303.
(35) Sanders, A. W.; Routenberg, D. A.; Wiley, B. J.; Xia, Y.; Dufresne, E. R.; Reed, M. A. Observation of Plasmon Propagation, Redirection, and Fan-Out in Silver Nanowires. *Nano Lett.* **2006**, *6*, 1822–1826.
(36) Barnes, W. L.; Dereux, A.; Ebbesen, T. W. Surface Plasmon Subwavelength Optics. *Nature* **2003**, *424*, 824–830.
(37) Xiong, Y.; Washio, I.; Chen, J.; Sadilek, M.; Xia, Y. Trimeric Clusters of Silver in Aqueous $AgNO_3$ Solutions and Their Role as Nuclei in Forming Triangular Nanoplates of Silver. *Angew. Chem. Int. Ed.* **2007**, *46*, 4917–4921.

AR7000974